Open Access Online Journal on Astronomy and Astrophysics

Acta Astrophysica Taurica

www.astrophysicatauricum.org

Acta Astrophys. Tau. 3(1), 39–43 (2022) doi:10.31059/aat.vol3.iss1.pp39-43

The morphology-dependent black hole–host galaxy correlations: a consequence of physical formation processes

Nandini Sahu[1,2], Alister W. Graham[2], and Benjamin L. Davis[3]

[1] OzGrav-Swinburne, Centre for Astrophysics and Supercomputing, Swinburne University of Technology, Hawthorn, VIC 3122, Australia
e-mail: nsahu@swin.edu.au

[2] Centre for Astrophysics and Supercomputing, Swinburne University of Technology, Hawthorn, VIC 3122, Australia
e-mail: agraham@swin.edu.au

[3] Center for Astro, Particle, and Planetary Physics (CAP 3), New York University Abu Dhabi
e-mail: ben.davis@nyu.edu

Submitted on November 23, 2021

ABSTRACT

For decades, astronomers have been investigating how the central supermassive black hole (BH) may govern the host galaxy's properties and *vice versa*. Our work adds another step to this study. We have performed state-of-the-art 2D modeling and multi-component photometric decompositions of the largest-to-date sample of galaxies with dynamically-measured black hole masses ($M_{\rm BH}$). The multi-component decomposition allows us to accurately extract the bulge (spheroid) stellar luminosity/mass and structural parameters (also for other galaxy components) and provides detailed galaxy morphologies. We investigated the correlations between $M_{\rm BH}$ and various host galaxy properties, including the bulge ($M_{*,\rm sph}$) and total galaxy ($M_{*,\rm gal}$) stellar masses discussed here. Importantly, we analyzed the role of galaxy morphology in these correlations. Our work reveals that the BH scaling relations depend on galaxy morphology and thus depend on the galaxy's formation and evolution physics. Here we discuss that in the $M_{\rm BH}$–$M_{*,\rm sph}$ diagram, early-type galaxies (ETGs) with a disk, ETGs without a disk, and late-type galaxies (LTG-spirals) define distinct relations, with quadratic slopes but different zero-points. We also review the $M_{\rm BH}$–$M_{*,\rm gal}$ relation, where ETGs and LTGs define different relations. Notably, the existence of the $M_{\rm BH}$–$M_{*,\rm gal}$ relations enables one to quickly estimate $M_{\rm BH}$ in other galaxies without going through the multi-component decomposition process to obtain $M_{*,\rm sph}$. The final morphology-dependent black hole scaling relations provide tests for morphology-aware simulations of galaxies with a central BH and hold insights for BH-galaxy co-evolution theories based on BH accretion and feedback.

Key words: Early-type galaxies (429) – Galaxy evolution (594) – Galaxy spheroids (2032) – Late-type galaxies (907) – Scaling relations (2031) – Supermassive black holes (1663)

1 Introduction

Almost all galaxies in the Universe are expected to host a supermassive black hole (BH) at their center, which is thought to co-evolve with the host galaxy (Lynden-Bell, 1969; Lynden-Bell and Rees, 1971). Plausibly, a galaxy may control the central BH's mass growth as the BH feeds on it. Conversely, the BH feedback is invoked to suggest that BH outflows expel out the gas content of the host galaxy, thereby shut down the star formation and regulate the galaxy's stellar content and other properties (e.g., Silk and Rees, 1998; Fabian, 1999). The observed correlations between BH mass and the host galaxy properties hold crucial insights for understanding this co-evolution. A review on various past efforts for establishing the correlation between BH mass and host galaxy properties (e.g., bulge mass, velocity dispersion, etc.), starting with the first studies and subsequent crucial advancements until 2016 can be found in Graham (2016).

The largest-to-date sample of galaxies with directly-measured black hole masses ($M_{\rm BH}$) currently numbers to 145 (listed in Sahu et al., 2019b). The direct BH mass measurement methods are proper motion, stellar and gas dynamical modeling, megamaser kinematics, and recent direct imaging. An informative review on the first four methods can be found in Ferrarese and Ford (2005), also see Peterson (2014), and the details about the recent direct-imaging technique can be found in Event Horizon Telescope Collaboration et al. (2019).

Savorgnan and Graham (2016), Davis et al. (2019), and Sahu et al. (2019a) collectively performed state-of-the-art two-dimensional modeling and multi-component decomposition of the host galaxy images of 123 of these galaxies. We did not simply add Sérsic functions (Sérsic, 1963, 1968), but fit for disks, bars, ansae, rings, etc., as required and revealed through both images and kinematics. The multi-component decomposition enabled us to extract the lumi-

nosity (and steller mass) associated with each component present in the galaxies, including the bulge (*also known as* the spheroid) and provided us with the structural parameters of galaxy components (e.g., central concentration/density, shape, and effective size of bulges, disks, bars, etc.). A detailed description of the above processes and the calculation of the bulge stellar mass ($M_{*,\rm sph}$) and also the total galaxy stellar mass ($M_{*,\rm gal}$) is presented in Sahu et al. (2019a).

In addition to the host galaxy properties, the multi-component decomposition provided us with the detailed morphology of the host galaxies, which proved to be crucial for our exploration of the BH scaling relations, providing a breakthrough, as discussed in the next Section 2. The morphology of galaxies in our sample can be broadly categorized into the early-type galaxies (ETGs) and the late-type galaxies (LTGs). The ETGs are comprised of almost pure spheroidal elliptical (E-type) galaxies, lenticular (S0-type) galaxies with large-scale rotating stellar disks in addition to the spheroid and other possible components, and ellicular (ES-type) galaxies with an intermediate-scale disk enclosed within their spheroids (Liller, 1966; Graham et al., 2016). LTGs are comprised of the spiral (S) galaxies, with spiral arms in their disks, in addition to the bulge and frequently seen bars, etc. The ETG and LTG terminology is simply followed from the Hubble's tuning fork sequence (Hubble, 1926), this classification does not represent a temporal evolution sequence of galaxies. Graham (2019) provides a compact morphology classification grid capturing the different galaxy types, including the typically overlooked ES galaxies.

The dataset used in the scaling diagrams shown in the following Section 2 along with the detailed morphology, are tabulated in the already published parent works of Savorgnan and Graham (2016), Davis et al. (2019), and Sahu et al. (2019a) which (collectively) performed the image analysis of the sample (as briefly described above). These three papers also present the directly measured central BH masses of the galaxies in our sample, along with their sources.

2 The black hole mass scaling relations

We have investigated the correlation between $M_{\rm BH}$ and various host galaxy properties, e.g., spheroid stellar mass ($M_{*,\rm sph}$, Sahu et al., 2019a), galaxy stellar mass ($M_{*,\rm gal}$, Sahu et al., 2019a), central stellar velocity dispersion of the galaxy (σ, Sahu et al., 2019b), spheroid central light concentration ($n_{\rm sph}$, Sahu et al., 2020), spheroid effective size ($R_{\rm e,sph}$, Sahu et al., 2020), spheroid projected luminosity/mass density ($\mu_{\rm sph}$ or $\Sigma_{\rm sph}$, Sahu et al., 2021), and spheroid internal density at various radii ($\rho_{\rm sph}$, Sahu et al., 2021). In all these diagrams, we paid special attention to finding out whether the BH scaling relations depend on the host galaxy morphology and, if so, the possible reason behind that. Here, we will only discuss the correlations between $M_{\rm BH}$ and the spheroid and total galaxy stellar masses.

All these correlations are obtained by performing a symmetric[1] Bivariate Correlated Errors and Intrinsic Scatter (BCES)[2] linear regression (Akritas and Bershady, 1996) and also cross-checked with the symmetric application of the modified FITEXY regression (Press et al., 1992; Tremaine et al., 2002; Markwardt, 2012). These regressions take into account the measurement errors in both the variables, allow for the intrinsic scatter in the data, and minimize the offset equally in both the ordinate and abscissa (see a comparison in Novak et al., 2006). The reason for preferring a symmetric regression is to avoid any biases upon assuming the galaxy property as an independent variable and the BH mass as a dependent variable or *vice versa*. In comparison to an asymmetric regression which only minimizes the vertical offsets between the data and the fitted regression line, the symmetric regression also provides a less biased/skewed extrapolation beyond the current range of the data.

2.1 Black hole mass versus bulge stellar mass

Our investigation into the correlation between BH mass and the host spheroid mass revealed that the $M_{\rm BH}$–$M_{*,\rm sph}$ relation is non-linear and, importantly, has morphology-dependent substructures (or divisions). In the $M_{\rm BH}$–$M_{*,\rm sph}$ diagram, we initially observed that ETGs and LTGs define different relations, as shown in the left-hand panel of Fig. 1. ETGs define a power-law, $M_{\rm BH} \propto M_{*,\rm sph}^{1.27\pm0.07}$ (Sahu et al., 2019a), while the LTGs define a steeper power-law, $M_{\rm BH} \propto M_{*,\rm sph}^{2.16\pm0.32}$ (Davis et al., 2019). The following full expressions of these relations are taken from (Sahu et al., 2019a, their Equations 10 and 16, respectively).

The best-fit relation obtained for all ETGs is given by

$$\log\left(\frac{M_{\rm BH}}{\rm M_\odot}\right) = (1.27\pm0.07)\log\left(\frac{M_{*,\rm sph}}{5\times10^{10}\,\rm M_\odot}\right) + (8.41\pm0.06), \quad (1)$$

with the total (intrinsic scatter plus measurement error) rms scatter $\Delta_{\rm rms|BH} = 0.52$ dex in the $M_{\rm BH}$-direction and a total orthogonal scatter of $\Delta_{\rm rms,\perp} = 0.32$ dex in the perpendicular direction. However, as we will soon see, this well-known relation, with a slope of $\sim$1 when a non-symmetric regression is used, appears to have been misleading and is physically meaningless.

The relation defined by the LTGs is given by

$$\log\left(\frac{M_{\rm BH}}{\rm M_\odot}\right) = (2.16\pm0.32)\log\left(\frac{M_{*,\rm sph}}{5\times10^{10}\,\rm M_\odot}\right) + (8.58\pm0.22), \quad (2)$$

with a total vertical scatter of $\Delta_{\rm rms|BH} = 0.64$ dex and an orthogonal scatter of $\Delta_{\rm rms,\perp} = 0.27$ dex.

The relation obtained for ETGs is superficial because the ETG sample has an internal offset between the ETGs with a (significant) disk component (i.e., ES- and S0-type galaxies) and ETGs without a disk (i.e., spheroidal E-type galaxies) in the $M_{\rm BH}$–$M_{*,\rm sph}$ diagram. As shown in the right-hand panel of Fig. 1, we find that ES/S0-type (shown in

[1] A symmetric regression provides a best-fit line which bisects the best-fit line obtained by Y-over-X (minimizes the offset in the vertical-direction and produces a shallower slope) or X-over-Y (minimizes the offset in the horizontal-direction and produces a steeper slope) regression.

[2] We used the PYTHON module from Nemmen et al. (2012), which is available at https://github.com/rsnemmen/BCES.

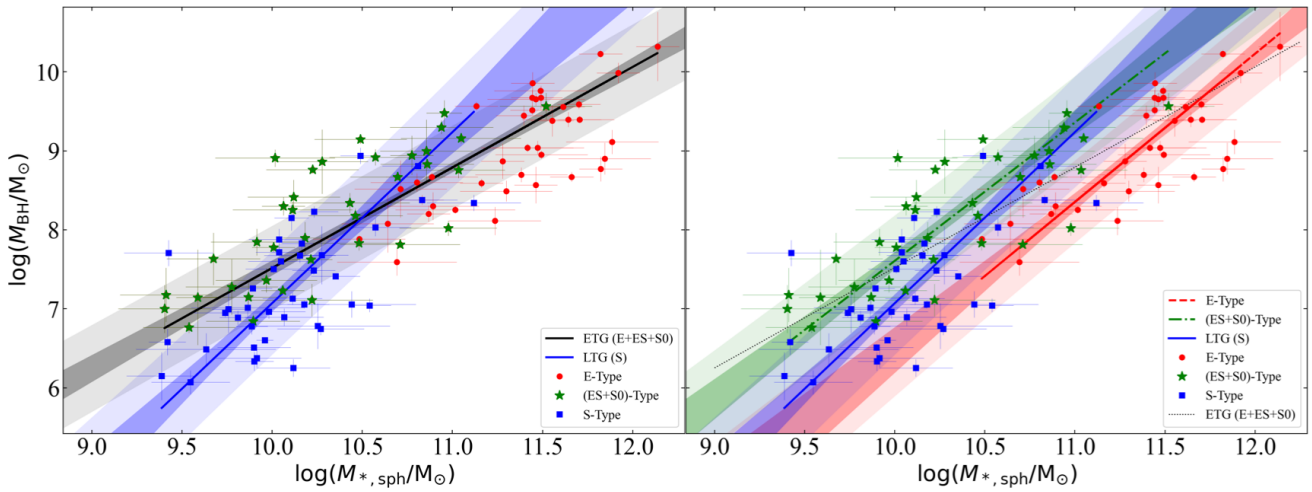

Fig. 1. Black hole mass versus spheroid stellar mass. The left-hand panel shows the black and blue best-fit lines for ETGs (ES/S0+E) and LTGs (S), respectively. The right-hand panel reveals the offset between the ETG subpopulations (E-type in red and ES/S0-types in green), defining almost parallel but offset M_{BH}–$M_{*,sph}$ relations, and retains the relation obtained for LTGs. Overall, S-, ES/S0-, and E-type galaxies have three distinct relations in the M_{BH}–$M_{*,sph}$ diagram, with almost quadratic slopes but different intercepts (see Equations 2, 3, and 4). The dark shaded region around the best-fit lines shows the $\pm1\sigma$ bound of their slopes and intercepts, and the light shaded region outlines the $\pm1\sigma$ scatter in each sample.

green) and E-type (shown in red) galaxies follow different M_{BH}–$M_{*,sph}$ relations which are almost parallel with slopes 1.86±0.20 and 1.90±0.20, respectively, but offset by 1.12 dex in the M_{BH}-direction (Sahu et al., 2019a). These relations, as provided below (Sahu et al., 2019a, their Equations 12 and 13, respectively), are steeper than the single relation obtained for the whole ETG sample (the dashed black line in the right-hand panel of Fig. 1) and have a slope which is comparable to that observed for the bulges of spiral galaxies.

The relation defined by ES- and S0-type galaxies is

$$\log\left(\frac{M_{BH}}{M_\odot}\right) = (1.86\pm0.20)\log\left(\frac{M_{*,sph}}{5\times10^{10}\,M_\odot}\right) + (8.90\pm0.13), \quad (3)$$

which has a vertical scatter of $\Delta_{rms|BH} = 0.57$ dex and an orthogonal scatter of $\Delta_{rms,\perp} = 0.27$ dex. The E-type galaxies define the following relation,

$$\log\left(\frac{M_{BH}}{M_\odot}\right) = (1.90\pm0.20)\log\left(\frac{M_{*,sph}}{5\times10^{10}\,M_\odot}\right) + (7.78\pm0.15), \quad (4)$$

with $\Delta_{rms|BH} = 0.50$ dex and orthogonal scatter $\Delta_{rms,\perp} = 0.23$ dex.

While the slopes of the M_{BH}–$M_{*,sph}$ relation for ETGs with a disk and ETGs without a disk are similar to that for LTGs (consistent within $\pm1\sigma$ error-bar on the slopes), the intercepts are different. Moreover, the single slope obtained for a sample of ETGs depends on the relative numbers of ETGs with and without a disk in one's sample. The familiar near-linear relation, which has hovered around 0.9 to 1.3 in the literature, is due to the sample selection. Furthermore, the practice of excluding the lower mass bulges in LTGs, under the banner that they are "pseudobulges," appears to be subjective pruning of systems following a near-quadratic relation. The practice of taking only the bright LTG bulges that overlap with the superficial near-linear relation (for blended samples of E and ES/S0 galaxies) appears to be an example of artificial reinforcement of the near-linear distribution.

For the bulk of the sample, we were able to perform our analysis using 3.6 μm Spitzer data, for which the stellar mass-to-light ratio, assumed to be constant at 0.60 (Meidt et al., 2014) for ETGs and 0.45 ± 0.07 for LTGs[3] (Querejeta et al., 2015; Davis et al., 2019), is well constrained. In the future, with individual bulge-specific M/L ratios, we will explore if the relation for the spiral galaxies becomes less steep and matches better with the relation for S0/ES galaxies (Fig. 1, right-hand panel).

Assuming a BH-bulge/galaxy co-evolution according to the M_{BH}–$M_{*,sph}$ relation, the steeper than linear relation for all galaxy types suggests that the growth rate in M_{BH} is larger than the stellar mass growth rate of the host bulge. As the zero-points of the relations are different, for a given bulge stellar mass, $M_{*,sph}$, the three relations will estimate different values of M_{BH}. Thus, one needs to be aware of the galaxy morphology and apply the corresponding scaling relation to obtain an accurate prediction of M_{BH} using the bulge mass. Interestingly, in a subsequent study of BH-galaxy evolution using a simulation, Marshall et al. (2020) also reported a similar offset between bulge-dominated and disk-dominated galaxies in the M_{BH}–$M_{*,sph}$ diagram.

The reason behind this offset between the ETGs with and without a disk is understood, and its origin has been further proven in Sahu et al. (2020, 2021). As evident in the M_{BH}–$M_{*,sph}$ diagram itself, the ES- and S0-type galaxies have a smaller $M_{*,sph}$ relative to that of E-type galaxies hosting the same central M_{BH}, causing this offset. The

[3] The stellar mass-to-light ratio for LTGs is reduced by 25% to correct for dust illumination in the near infrared band, see Davis et al. (2019) for more details.

ES- and S0-type galaxies have two dominant components, the bulge, and the disk, in addition to other relatively less massive/dominant components; thus, their total galaxy stellar mass is predominantly contributed by the bulge plus the disk. However, E-type galaxies are spheroid dominant, and thus their total galaxy stellar mass is close to the spheroid stellar mass. The lenticular galaxies have bulge-to-total luminosity/mass ratios of 1/4 (Laurikainen et al., 2005; Graham and Worley, 2008) and a major merger of two lenticular (or ellicular) galaxies will cause a shift towards the $M_{\rm BH}$–$M_{*,\rm sph}$ relation for elliptical galaxies.

The realization of this offset also implied that a more generalized relation might exist between $M_{\rm BH}$ and total galaxy stellar mass, $M_{*,\rm gal}$, which can unite all ETGs with and without a disk. The use of an $M_{\rm BH}$–$M_{*,\rm gal}$ relation would also apply to rare but identified bulge-less galaxies (see Davis et al., 2018; Davis et al., 2019, for some examples).

2.2 Black hole mass versus galaxy stellar mass

Upon analyzing the distribution of galaxies in the BH mass versus total galaxy stellar mass diagram, we observed that the ES- and S0-type galaxies shift (right) towards the E-type galaxies as the mass of other components, especially the disk, is now accounted for in the galaxy stellar mass of ES- and S0-types. Thus, in the $M_{\rm BH}$–$M_{*,\rm gal}$ diagram, the offset between the ETGs with a disk and ETGs without a disk fades, suggesting a single relation for all (E+ES+S0) ETGs, as shown by the black line in Fig. 2. This relation for ETGs (Equation 11 of Sahu et al., 2019a) is given by

$$\log\left(\frac{M_{\rm BH}}{\rm M_\odot}\right) = (1.65\pm0.11)\log\left(\frac{M_{*,\rm gal}}{5\times10^{10}\,\rm M_\odot}\right)+(8.02\pm0.08). \quad (5)$$

The distribution of ETGs about this line has $\Delta_{\rm rms|BH}$ = 0.58 dex in the $M_{\rm BH}$-direction and an orthogonal scatter of $\Delta_{\rm rms,\perp}$ = 0.30 dex. The scatter here is only slightly higher than that of the E-types alone, and it is comparable to that of the ES/S0-types in the $M_{\rm BH}$–$M_{*,\rm sph}$ diagram. Furthermore, it is not much higher than the scatter in the $M_{\rm BH}$–σ diagram for ETGs (0.44 dex, Sahu et al., 2019b).

Upon including the spiral galaxies (LTGs) in the $M_{\rm BH}$–$M_{*,\rm gal}$ diagram, they are found to define a much steeper relation with a power-law slope twice as that of ETGs. The relation for LTGs obtained in Davis et al. (2018), also shown here in Fig. 2 color-coded in green, can be expressed as

$$\log\left(\frac{M_{\rm BH}}{\rm M_\odot}\right) = (3.05\pm0.70)\log\left(\frac{M_{*,\rm gal}}{5\times10^{10}\,\rm M_\odot}\right)+(6.93\pm0.14). \quad (6)$$

The vertical scatter in the distribution of LTGs about this line is $\Delta_{\rm rms|BH}$ = 0.79 dex and the orthogonal scatter is $\Delta_{\rm rms,\perp}$ = 0.25 dex, comparable to the orthogonal scatter (0.27 dex) about the $M_{\rm BH}$–$M_{*,\rm sph}$ relation for LTGs. The steeper $M_{\rm BH}$–$M_{*,\rm gal}$ relation relative to the $M_{\rm BH}$–$M_{*,\rm sph}$ relation for spiral galaxies is because of the decreasing trend of the bulge-to-total ratio (or equivalently the increasing total-to-bulge ratio) while traversing from early-to-late (i.e., Sa/Sb to Sc/Sd) type spiral galaxies.

The essential message of presenting the $M_{\rm BH}$–$M_{*,\rm gal}$ diagram here is that there exists a correlation between the BH mass and the total host galaxy stellar mass. Moreover, the morphology-dependent $M_{\rm BH}$–$M_{*,\rm gal}$ relations can directly be used to estimate the BH mass using total galaxy stellar mass, without going through the rigorous multi-component decomposition of a galaxy to extract the mass of its bulge.

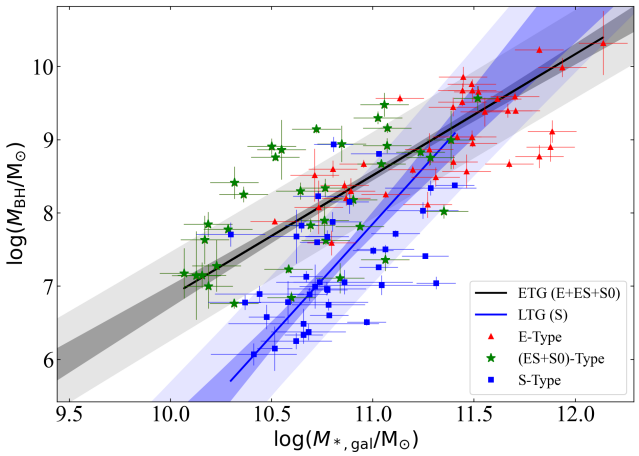

Fig. 2. Black hole mass versus total galaxy stellar mass. This diagram has two distinct relations defined by (all) ETGs and LTGs (see Equations 5 and 6).

3 Discussion

In addition to the morphology-dependent $M_{\rm BH}$–$M_{*,\rm sph}$ and $M_{\rm BH}$–$M_{*,\rm gal}$ relations reviewed here, we have also revealed morphology-dependent $M_{\rm BH}$–spheroid central concentration (i.e., Sérsic index), $M_{\rm BH}$–spheroid effective sizes, $M_{\rm BH}$–spheroid surface brightness (and projected mass density), and $M_{\rm BH}$–spheroid internal mass density relations (see Sahu et al., 2020, 2021). These diagrams also host and explain the substructures based on galaxy morphology seen in the $M_{\rm BH}$–$M_{*,\rm sph}$ diagram, and provide alternatives to predict BH hole mass using various spheroid properties. We have also revealed the morphology-dependent division in the $M_{\rm BH}$–σ diagram, consistent with the division in the Luminosity–σ relation, using the current extended sample of 145 galaxies (see Sahu et al., 2019b).

The morphology categorizes the structural appearance of a galaxy, which is built through the formation and evolutionary processes the galaxy has undergone over cosmic time, and depends on many factors, e.g., initial density, angular momentum, the number density of galaxies around it, the properties of the intergalactic medium, and the feeding of gas and minor mergers, etc. This influences the feeding and growth of the BH and the stellar mass of the host galaxy. The dependence of BH scaling relations on the galaxy morphology suggests that the central BHs are conscious of the evolutionary track of the host galaxy, reinforcing the notion of BH–galaxy co-evolution, but requiring modification from the standard picture by introducing an awareness of morphology. Furthermore, past feedback schemes which produced or used a near-linear $M_{\rm BH}$–$M_{\rm bulge}$ relation require significant modification to conform with the observed near-quadratic relation

(see Graham and Scott, 2013, their Equation 9). Such a realization can be helpful for theoretical and analytical studies on BH–galaxy co-evolution, including the studies on BH feedback (King, 2010; Seymour et al., 2012; Volonteri and Ciotti, 2013; Heckman and Best, 2014; Habouzit et al., 2019; Dekel et al., 2019).

The revised black hole-galaxy correlations can be used to test the validity of simulations trying to form galaxies with BHs at their centers (e.g., Croton et al., 2006; Schaye et al., 2015; Hopkins et al., 2018). In future work, morphology-dependent scaling relations will be used by us to obtain morphology-aware virial factors required in the reverberation mapping technique and Dibai's single epoch spectrum method (Dibai, 1977) to calculate BH mass in active galactic nuclei (Sergeev et al., 2007; Bochkarev and Gaskell, 2009; Denney et al., 2010; Bentz and Manne-Nicholas, 2018). These relations can also provide modified and morphology-aware BH mass functions and can improve the predictions for the amplitude and frequency of the long-wavelength gravitational waves searched for by pulsar timing arrays and future space interferometers (Chen et al., 2019).

Acknowledgements. This research was supported under the Australian Research Council's funding scheme DP17012923 and CE170100004.

References

Akritas M.G., Bershady M.A., 1996. Astrophys. J., vol. 470, p. 706.
Bentz M.C., Manne-Nicholas E., 2018. Astrophys. J., vol. 864, 146.
Bochkarev N.G., Gaskell C.M., 2009. Astronomy Letters, vol. 35, no. 5, pp. 287–293.
Chen S., Sesana A., Conselice C.J., 2019. Mon. Not. Roy. Astron. Soc., vol. 488, no. 1, pp. 401–418.
Croton D.J., Springel V., White S.D.M., et al., 2006. Mon. Not. Roy. Astron. Soc., vol. 365, pp. 11–28.
Davis B.L., Graham A.W., Cameron E., 2018. Astrophys. J., vol. 869, 113.
Davis B.L., Graham A.W., Cameron E., 2019. Astrophys. J., vol. 873, no. 1, p. 85.
Dekel A., Lapiner S., Dubois Y., 2019. arXiv e-prints, arXiv:1904.08431.
Denney K.D., Peterson B.M., Pogge R.W., et al., 2010. Astrophys. J., vol. 721, no. 1, pp. 715–737.
Dibai E.A., 1977. Soviet Astronomy Letters, vol. 3, pp. 1–3.
Event Horizon Telescope Collaboration, Akiyama K., Alberdi A., et al., 2019. Astrophys. J., vol. 875, no. 1, L6.
Fabian A.C., 1999. Mon. Not. Roy. Astron. Soc., vol. 308, pp. L39–L43.
Ferrarese L., Ford H., 2005. Space Sci. Rev., vol. 116, pp. 523–624.
Graham A.W., 2016. In E. Laurikainen, R. Peletier, D. Gadotti (Eds.), Galactic Bulges. Astrophysics and Space Science Library, vol. 418, p. 263. doi:10.1007/978-3-319-19378-6_11 (arXiv:1501.02937).
Graham A.W., 2019. Mon. Not. Roy. Astron. Soc., p. 1547.
Graham A.W., Ciambur B.C., Savorgnan G.A.D., 2016. Astrophys. J., vol. 831, 132.
Graham A.W., Scott N., 2013. Astrophys. J., vol. 764, 151.
Graham A.W., Worley C.C., 2008. Mon. Not. Roy. Astron. Soc., vol. 388, pp. 1708–1728.
Habouzit M., Genel S., Somerville R.S., et al., 2019. Mon. Not. Roy. Astron. Soc., vol. 484, no. 4, pp. 4413–4443.
Heckman T.M., Best P.N., 2014. Ann. Rev. Astron. Astrophys., vol. 52, pp. 589–660.
Hopkins P.F., Wetzel A., Kereš D., et al., 2018. Mon. Not. Roy. Astron. Soc., vol. 480, no. 1, pp. 800–863.
Hubble E.P., 1926. Astrophys. J., vol. 64, pp. 321–369.
King A.R., 2010. Mon. Not. Roy. Astron. Soc., vol. 402, no. 3, pp. 1516–1522.
Laurikainen E., Salo H., Buta R., 2005. Mon. Not. Roy. Astron. Soc., vol. 362, pp. 1319–1347.
Liller M.H., 1966. Astrophys. J., vol. 146, p. 28.
Lynden-Bell D., 1969. Nature, vol. 223, pp. 690–694.
Lynden-Bell D., Rees M.J., 1971. Mon. Not. Roy. Astron. Soc., vol. 152, p. 461.
Markwardt C., 2012. MPFIT: Robust non-linear least squares curve fitting (ascl:1208.019).
Marshall M.A., Mutch S.J., Qin Y., Poole G.B., Wyithe J.S.B., 2020. Mon. Not. Roy. Astron. Soc., vol. 494, no. 2, pp. 2747–2759.
Meidt S.E., Schinnerer E., van de Ven G., et al., 2014. Astrophys. J., vol. 788, 144.
Nemmen R.S., Georganopoulos M., Guiriec S., et al., 2012. Science, vol. 338, p. 1445.
Novak G.S., Faber S.M., Dekel A., 2006. Astrophys. J., vol. 637, no. 1, pp. 96–103.
Peterson B.M., 2014. Space Sci. Rev., vol. 183, no. 1-4, pp. 253–275.
Press W.H., Teukolsky S.A., Vetterling W.T., Flannery B.P., 1992. Numerical recipes in FORTRAN. The art of scientific computing.
Querejeta M., Meidt S.E., Schinnerer E., et al., 2015. Astrophys. J., Suppl. Ser. , vol. 219, 5.
Sahu N., Graham A.W., Davis B.L., 2019a. Astrophys. J., vol. 876, no. 2, 155.
Sahu N., Graham A.W., Davis B.L., 2019b. Astrophys. J., vol. 887, no. 1, 10.
Sahu N., Graham A.W., Davis B.L., 2020. Astrophys. J., vol. 903, no. 2, 97.
Sahu N., Graham A.W., Davis B.L., 2021. Astrophys. J., vol. submitted.
Savorgnan G.A.D., Graham A.W., 2016. Astrophys. J., Suppl. Ser. , vol. 222, 10.
Schaye J., Crain R.A., Bower R.G., et al., 2015. Mon. Not. Roy. Astron. Soc., vol. 446, no. 1, pp. 521–554.
Sergeev S.G., Klimanov S.A., Chesnok N.G., Pronik V.I., 2007. Astronomy Letters, vol. 33, no. 7, pp. 429–436.
Sérsic J.L., 1963. BAAA, vol. 6, p. 41.
Sérsic J.L., 1968. Tech. rep., Atlas de Galaxias Australes - English Translation of the chapter "Photometric Analysis". doi:10.5281/zenodo.2562394.
Seymour N., Altieri B., De Breuck C., et al., 2012. Astrophys. J., vol. 755, 146.
Silk J., Rees M.J., 1998. Astron. Astrophys., vol. 331, pp. L1–L4.
Tremaine S., Gebhardt K., Bender R., et al., 2002. Astrophys. J., vol. 574, pp. 740–753.
Volonteri M., Ciotti L., 2013. Astrophys. J., vol. 768, 29.